JOURNAL OF COMPUTATIONAL PHYSICS **130,** 148–159 (1997)
ARTICLE NO. CP965588

An Efficient Quantum Mechanical Method for the Electronic Dynamics of the Three-Dimensional Hydrogen Atom Interacting with a Linearly Polarized Strong Laser Pulse

Hirohiko Kono, Akihisa Kita, Yukiyoshi Ohtsuki, and Yuichi Fujimura

Department of Chemistry, Graduate School of Science, Tohoku University, Kawauchi North Campus, Kawauchi, Sendai 980-77, Japan
E-mail: kono@mcl.chem.tohoku.ac.jp

Received April 15, 1996

We present a method whereby the 3D dynamics of the electronic wave packet in a hydrogen atom can be calculated efficiently. The method is constructed so as to satisfy the following two requirements: the wave function is zero at the Coulomb singular point so that the numerical difficulties concerning the singularity are avoided; the coordinate system is chosen so that the differential operators in the Hamiltonian can be well evaluated by the 3-point finite difference formula even near the singular point. The generalized cylindrical coordinate system $(\xi^\lambda, z, \varphi)$ is introduced to satisfy the above conditions, and the value of λ is determined to be $\frac{3}{2}$. The Schrödinger equation is discretized in time and space and solved by the Peaceman–Rachford method. The $\lambda = \frac{3}{2}$ coodinate system helps the reduction in the number of grid points. To examine the numerical stability and accuracy of our method, we first apply it to cases where no laser field is turned on. The errors for the ordinary cylindrical coordinate system ($\lambda = 1$) are more than ten times as large as those for $\lambda = \frac{3}{2}$. We then apply the method to the case where the atom interacts with a linearly polarized strong laser pulse. Our method is highly reliable and is a powerful tool for analyzing ionization processes of the hydrogen atom. © 1997 Academic Press

1. INTRODUCTION

Femtosecond technology has opened up a new field of study regarding coherent electron motions such as the multiphoton ionization dynamics of atoms and molecules in strong laser fields [1–4] and the Kepler motion in Rydberg states [5]. To simulate these processes quantum-mechanically, one must cope with the Coulomb potential characterized by its long range and its singularity at the origin. The grid boundary in coordinate space must be chosen to be far from the origin to accommodate the wave function and the grid spacing must be small to adjust to the steep change of the Coulomb potential near the origin. In many cases, the numerical studies are thus limited to a one-dimensional atom (one electron) [1, 6–8]. It is still computationally demanding to deal with multidimensional Coulomb problems, although progress has been made toward the development of efficient time evolution methods [9–13]. The efficient method for the Coulomb problem has not been established yet, in spite of its pressing need.

Various time evolution methods have been proposed such as the kinetic referenced split operator method (KRSO) [14–16], the Cayley–Cranck–Nicholson method (CCN) [17, 18], and the Peaceman–Rachford method (PR) [19, 20] (which is a two-dimensional version of the alternating-direction implicit method [21, 22]). In these methods, to advance the wave function at time t to the next time step $t + \Delta t$ (where Δt is the time spacing), an approximate short time propagator is operated on the wave function. These three methods use different types of approximate propagators. The three approximate propagators have the same accuracy of order Δt^2 and are unitary so that the norm is strictly conserved; they are applicable to the time-dependent Hamiltonian, which suits the purpose of describing the dynamical behavior of atoms and molecules interacting with laser pulses. These methods are, however, different in efficiency and accuracy (which depends on the potential [16]).

In order to accelerate the study of the dynamics involving Rydberg-like or continuum states and to facilitate the simulation of multidimensional problems, first of all, it is necessary to know which time evolution method is the best for the one-dimensional Coulomb problem and what kind of improvement (e.g., variable transformation) can be made. In a previous paper [23], we have applied these methods to the one-dimensional radial Coulomb problem. Calculating the time evolutions of nonstationary states, we have compared them in efficiency and accuracy.

The comparative study has shown that for the Coulomb potential the KRSO is inferior to the other two methods. First, the time spacing required for the achievement of high accuracy is extremely small. Second, as the number of grid points N increases (the grid spacing in coordinate space decreases), the error in coordinate space decreases but the error in momentum space bounces up after it reaches the minimum (the error turnover). The instability of the KRSO is attributed to the contamination with continuum states of high momenta (which is induced by the error terms of inverse powers of the radial coordinate r).

0021-9991/97 $25.00
Copyright © 1997 by Academic Press
All rights of reproduction in any form reserved.

We have concluded that the KRSO is not suitable for the Coulomb problems (although it is very powerful for nonsingular internuclear potentials). The CCN which is unconditionally stable and consistent is found to be most efficient and computationally less demanding. Use of larger time steps is allowed. The PR, which plays the major role in multidimensional Coulomb problems as will be shown in this paper, becomes equivalent to the CCN at a little expense. For the CCN and the PR, the accuracy is greatly improved by variable transformations [24–26], which helps the reduction in the number of grid points.

In this paper, we report a new method whereby the 3D dynamics of the electronic wave packet in a hydrogen atom can be simulated on the condition that an axis component of the angular momentum is conserved. We would like to construct a new method that satisfies the following two requirements: (i) the wave function is transformed so that it is zero at the Coulomb singular point (which ensures that the numerical difficulties concerning the singularity are avoided); (ii) the coordinate system is chosen so that the differential operators in the Hamiltonian can be well evaluated by the 3-point finite difference formula even near the singular point.

The cylindrical coordinate system (ρ, z, φ), which has been mostly used to represent the time-dependent Hamiltonian for the hydrogen atom [10, 11], does not meet the second requirement. The choice of coordinate systems is crucial [27]. In this paper, we here propose the generalized cylindrical coordinate system (ξ^λ, z, φ). The value of λ is determined so that the above two requirements are fulfilled. The new Schrödinger equation, represented in terms of the wave function transformed and the corresponding Hamiltonian, is solved by the PR method.

To examine the numerical stability and accuracy of our method, we first apply it to cases where no laser field is turned on. The wave functions calculated by our method are compared with the exact ones to estimate the errors. It is also examined whether the stability and the consistency with the Schrödinger equation are conditional or unconditional. Convergence is tested by reducing the time step Δt and the grid spacings Δz and $\Delta\xi$. Our method is then applied to the case where the electric field of the pulse is linearly polarized. The z-axis can be chosen to be the direction of the electric field: the problem has cylindrical symmetry and the z-component of the angular momentum is conserved. The 3D problem is thus reduced to the 2D problem. We illustrate a series of snapshots of the electronic wave packet that moves in real space while coherently interacting with a strong femtosecond laser pulse.

2. THE PEACEMAN–RACHFORD METHOD (PR)

The time evolution of a quantum mechanical system is governed by the Schrödinger equation (atomic units are used throughout this paper, unless otherwise indicated),

$$i\frac{\partial}{\partial t}\psi = H(t)\psi, \tag{1}$$

where $H(t)$ is the time dependent Hamiltonian of the system. If the system is in state $\psi(t_0)$ at time t_0, the formal solution of Eq. (1) is expressed as

$$\psi(t) = U(t, t_0)\psi(t_0), \tag{2}$$

where using the time ordering operator $\hat{\mathrm{T}}$ the time propagator $U(t, t_0)$ is given by

$$U(t, t_0) = \hat{\mathrm{T}} \exp\left[-i\int_{t_0}^{t} H(t')\,dt'\right]. \tag{3}$$

When the Hamiltonian is time independent, $U(t, t_0) = \exp[-i(t - t_0)H]$.

If the time step Δt is sufficiently small, the short time propagator $U(t + \Delta t, t)$ can be replaced with an approximate propagator that is accurate up to a certain order of Δt. The wave function at the desired time is obtained by operating such an approximate propagator on the wave function iteratively. In the following, we briefly review two approximate methods; the Cayley–Cranck–Nicholson method (CCN) and a more versatile one, namely, the PR method. The latter is regarded as the two-dimensional version of the alternating-direction implicit method (ADI) which is applicable to multidimensional Coulomb problems.

The CCN is based on the following approximate propagator called the Cayley form [17, 18]

$$\mathrm{e}^{-iH\Delta t} \approx \frac{1 - iH\,\Delta t/2}{1 + iH\,\Delta t/2}. \tag{4}$$

We take the time evolution of the hydrogen atom with zero angular momentum as an example to outline the CCN

$$i\frac{\partial}{\partial t}R_{\mathrm{S}} = \left\{-\frac{1}{2r^2}\frac{\mathrm{d}}{\mathrm{d}r}r^2\frac{\mathrm{d}}{\mathrm{d}r} - \frac{1}{r}\right\}R_{\mathrm{S}}, \tag{5}$$

where R_{S} is the radial wave function of the azimuthal quantum number $l = 0$ (a linear combination of $l = 0$ states) and no time-dependent perturbations are present. For the transformed wave function

$$\psi = rR_{\mathrm{s}}, \tag{6}$$

the transformed Hamiltonian H that satisfies the form of Eq. (1) is given by

$$H = K + V, \tag{7}$$

where K is the kinetic energy operator and V is the Coulomb potential:

$$K = -\frac{1}{2}\frac{d^2}{dr^2}; \quad V = -\frac{1}{r}. \tag{8}$$

In the following, we take advantage of the boundary condition that ψ is zero at the singular point $r = 0$.

Using the Cayley form, the wave function at time $t_n = n\,\Delta t + t_0$, ψ^n, can be advanced by the following implicit scheme called the Cranch–Nicholson scheme [18],

$$\begin{aligned} &-\frac{i\,\Delta t}{4\,\Delta r^2}\psi_{j+1}^{n+1} + \left\{1 + \frac{i\,\Delta t}{2\,\Delta r^2} + \frac{i\,\Delta t}{2}V(r_j)\right\}\psi_j^{n+1} \\ &-\frac{i\,\Delta t}{4\,\Delta r^2}\psi_{j-1}^{n+1} = +\frac{i\,\Delta t}{4\,\Delta r^2}\psi_{j+1}^{n} \\ &+\left\{1 - \frac{i\,\Delta t}{2\,\Delta r^2} - \frac{i\,\Delta t}{2}V(r_j)\right\}\psi_j^{n} + \frac{i\,\Delta t}{4\,\Delta r^2}\psi_{j-1}^{n}, \end{aligned} \tag{9}$$

where $\psi_j^n = \psi^n(r = r_j)$, Δr is the grid spacing, and the 3-point finite difference formula for the second derivative is used

$$\frac{\partial^2}{\partial r^2}\psi_j^n = \frac{\psi_{j+1}^n - 2\psi_j^n + \psi_{j-1}^n}{\Delta r^2} + O(\Delta r^2). \tag{10}$$

The system of an infinite number of linear equations is truncated with the two boundary conditions $\psi(r = 0) = 0$ and $\psi(r = L_0) = 0$, where the grid end L_0 is chosen so that the amplitude of $\psi(r)$ is negligible for $r > L_0$. The range $[0, L_0]$ is discretized by N grid points. The resultant tridiagonal system of $N - 2$ equations can be solved efficiently. It has been shown by the von Neumann analysis (and numerically) that the CNN is unconditionally stable and consistent. The error does not grow exponentially in time and the convergence to the solution of the Schrödinger equation is obtained by reducing Δr and Δt independently (without constraints).

Although the CCN has many advantages such as the conservation of energy, its direct application has been limited only to one- or two-dimensional problems. Note that the CCN is required to solve a system of linear equations at each time step. Even for the two-dimensional problem, the matrix of the system of equations is very large to invert and is not thin banded even if contractions are made on the indices of the matrix [18, 28] (the matrix representation for the two-dimensional case has four indices). The efficiency of computation is rather poor. It has, however, been known that the inefficiency of computation for multidimensional cases is cured by a different way of generalizing the Cranck–Nicholson algorithm, namely, the ADI [21, 22]. The ADI maintains the quality of the CCN (in one dimension) and each time step requires only the solutions of tridiagonal systems for reduced one-dimensional spaces.

The ADI embodies the powerful idea of operator splitting and time splitting. For instance, one can split the time evolution operator $\exp[-i(A + B)\,\Delta t]$, where A and B are arbitrary operators, by using the ADI as

$$e^{-i(A+B)\Delta t} \approx \frac{1}{1 + iA\,\Delta t/2}\frac{1 - iB\,\Delta t/2}{1 + iB\,\Delta t/2}(1 - iA\,\Delta t/2), \tag{11}$$

The above operation is separated into two implicit schemes by introducing an "artificial" intermediate state $\psi^{n+1/2}$,

$$(1 + iB\,\Delta t/2)\,\psi^{n+1/2} = (1 - iA\,\Delta t/2)\,\psi^n, \tag{12a}$$

$$(1 + iA\,\Delta t/2)\,\psi^{n+1} = (1 - iB\,\Delta t/2)\,\psi^{n+1/2}, \tag{12b}$$

which is known as the Peaceman–Rachford (PR) method [19, 20].

This two-step scheme is very useful for two-dimensional problems. Suppose that the operator A contains differential operators of coordinate x (it does not include those of coordinate y) and B contains those of coordinate y. As in the CCN, the 3-point finite difference formula can be used for the operation of differential operators on the wave functions. The PR method then reduces Eq. (11) to two sets of tridiagonal systems of equations: from Eq. (12a), a tridiagonal system of equations connecting the probability amplitudes at grid points $\{y_j\}$ is obtained at each x grid point; from Eq. (12b), a tridiagonal system of equations connecting the probability amplitudes at $\{x_j\}$ is obtained at each y. The whole system is therefore reduced to two sets of subsystems in one space dimension like Eq. (9). The tridiagonal systems of equations can be solved by setting $\psi(x, y) = 0$ at the appropriate boundaries.

3. TRANSFORMATION OF THE HAMILTONIAN AND WAVE FUNCTION

We apply the PR method for the simulation of the electron motion in the 3D hydrogen atom interacting with a linearly polarized laser pulse. To that end, we derive the Hamiltonian and wave function that can be treated in the framework of the PR method, on the assumption that the pulse is a plane wave (the electric field strength is assumed to be homogeneous along the direction of polarization of the light) and the dipole approximation is valid. If the polarization direction is chosen as the z-axis, the z-component of the angular momentum is conserved; i.e., the magnetic quantum number m is constant. Using cylindrical coordinates ρ, z, φ ($x = \rho\cos\varphi$, $y = \rho\sin\varphi$, $z = z$), the Schrödinger equation can then be written as

$$i\frac{\partial}{\partial t}R(\rho,z)=\left\{-\frac{1}{2\rho}\frac{\partial}{\partial\rho}\rho\frac{\partial}{\partial\rho}-\frac{1}{2}\frac{\partial^2}{\partial z^2}+\frac{m^2}{2\rho^2}-\frac{1}{\sqrt{\rho^2+z^2}}+z\mathscr{E}(t)\sin(\omega t)\right\}R(\rho,z), \tag{13}$$

where $\mathscr{E}(t)$ and ω are the electric field strength and frequency of the pulse, respectively. The total wave function is given by $R(\rho,z)e^{im\varphi}/\sqrt{2\pi}$ and the function $R(\rho, z)$ is normalized as

$$\int_0^\infty d\rho\int_{-\infty}^{\infty}dz\rho|R(\rho,z)|^2=1. \tag{14}$$

We plan to use the 3-point finite difference formula to evaluate the operation of the differential operators contained in the Hamiltonian. For the cylindrical coordinate system, the finite difference formula however does not give sufficient accuracy. It is crucial to seek out a coordinate system for the fine difference formula to work well. To find such a coordinate system, we propose the generalized cylindrical coordinate system as

$$x=\xi^\lambda\cos\varphi;\quad y=\xi^\lambda\sin\varphi;\quad z=z, \tag{15}$$

where λ is a parameter to be determined so that the finite difference formula works well ($\lambda=1$ leads to the ordinary cylindrical coordinates).

To avoid the numerical difficulties concerning the Coulomb singularity, the wave function $R(\xi, z)$ which is finite at the origin $r=0$ must be transformed to $\psi(\xi, z)$ that is zero at the origin. We further impose the following normalization condition on the transformed wave function $\psi(\xi, z)$

$$\int_0^\infty d\xi\int_{-\infty}^{\infty}dz|\psi(\xi,z)|^2=1. \tag{16}$$

Note that the volume element for normalization is $d\xi\,dz$, not like $\xi\,d\xi\,dz$. The meaning of this normalization condition will be discussed later.

The transformed wave function that satisfies the normalization condition (16) is uniquely determined as

$$\psi(\xi,z)=\sqrt{\lambda}\xi^{\lambda-1/2}R(\xi,z). \tag{17}$$

We will choose $\lambda>1/2$ so that the transformed wave function $\psi(\xi, z)$ satisfies the necessary condition that ψ is zero at the origin. Inserting Eq. (17) into Eq. (13), one obtains the transformed Hamiltonian that fulfills the form of Eq. (1).

$$H(t)=K_\xi+K_z+V_{\mathrm{E}}(t), \tag{18}$$

where

$$K_\xi=-\frac{1}{2\lambda^2\xi^{2\lambda}}\left\{\xi^2\frac{\partial^2}{\partial\xi^2}-2(\lambda-1)\xi\frac{\partial}{\partial\xi}+\left(\lambda-\frac{1}{2}\right)^2\right\}, \tag{19}$$

$$K_z=-\frac{1}{2}\frac{\partial^2}{\partial z^2}, \tag{20}$$

$$V_{\mathrm{E}}(t)=-\frac{1}{\sqrt{\xi^{2\lambda}+z^2}}+\frac{m^2}{2\xi^{2\lambda}}+z\mathscr{E}(t)\sin(\omega t). \tag{21}$$

The radial coordinate r is expressed as $(\xi^{2\lambda}+z^2)^{1/2}$.

We now apply the PR method to the time-evolution system of the above transformed Hamiltonian. The kinetic energy parts with respect to coordinates z and ξ in the time-dependent Hamiltonian $H(t)$ are separated into $A(t)$ and $B(t)$ as

$$A(t)=K_z+\tfrac{1}{2}V_{\mathrm{E}}(t) \tag{22}$$

and

$$B(t)=K_\xi+\tfrac{1}{2}V_{\mathrm{E}}(t). \tag{23}$$

The potential energy is divided into halves so that $A(t)\psi$ and $B(t)\psi$ vanish at the origin. This ensures that the boundary condition $\psi(r=0)=0$ is maintained not only for ψ^n but also for intermediate state $\psi^{n+1/2}$. To keep the accuracy of order Δt^2 in the PR method, A and B in the right-hand side of Eq. (11) must be replaced with those at the midpoint of the time step, $t_{n+1/2}=t_n+\Delta t/2$ (see Eq. (31)):

$$U(t+\Delta t,t)\approx\frac{1}{1+i\,\Delta tA(t_{n+1/2})/2}\frac{1-i\,\Delta tB(t_{n+1/2})/2}{1+i\,\Delta tB(t_{n+1/2})/2}\times[1-i\,\Delta tA(t_{n+1/2})/2]. \tag{24}$$

The operation is divided into two steps as in Eq. (12).

The boundary conditions imposed are as follows: (i) $\psi(\xi=0, z)=0$ (from the nature of the transformed wave function) and $\psi(\xi=\xi_{\max}, z)=0$; (ii) $\psi(\xi, z=-z_{\max})=\psi(\xi, z=z_{\max})=0$. The boundary lines at which $\psi(\xi, z)=0$ compose a square. The end points $\xi_{\max}$ and $z_{\max}$ are chosen so that $\psi(\xi, z)$ is negligible outside the square. The first boundary condition is used to obtain tridiagonal systems of equations from Eq. (12a); the second one is used to obtain tridiagonal systems of equations from Eq. (12b).

The value of λ has not been determined yet. Since λ must be greater than $\frac{1}{2}$, we start with the $\lambda=1$ coordinate system (the ordinary cylindrical coordinate system) which has been employed in the conventional time evolution method for the hydrogen atom. For this coordinate system, however, the finite difference formulae do not work well. Let us take the 1s function, for example. The leading term of ξ in $\psi_{1s}(\xi, z)$ near the origin is on the order of $\xi^{1/2}$. The

second derivative of $\xi^{1/2}$ is $-\xi^{-3/2}/4$, while the 3-point finite difference formula is $[(\xi + \Delta\xi)^{1/2} + (\xi - \Delta\xi)^{1/2} - 2\xi^{1/2}]/(\Delta\xi)^2$. The ratio of the latter to the former is 2.343, 1.090, and 1.037, at $\xi = \Delta\xi, 2\Delta\xi$, and $3\Delta\xi$, respectively. The difference at small ξ between the differential and the finite difference causes serious errors for the period of the wave packet dynamics (see Section 4B). The 5-point finite difference formula is even worse. No matter how small $\Delta\xi$ is, the derivatives at small ξ cannot be accurately evaluated by the finite difference formulae.

We next increase the value of λ to $\frac{3}{2}$. In this case, the leading term of ξ in $\psi_{1s}(\xi, z)$ near the origin is ξ and the first and second ξ-derivatives can, therefore, be evaluated accurately by 3-point finite difference formulae [29]. The second z-derivative is also evaluated accurately by the 3-point finite difference formula. Thereby, for example, the second z-derivative of $\psi_{1s}(\xi, z)$ is given exactly at the limit of $\Delta z \to 0$. It would be possible to prove that the derivatives of an arbitrary eigenfunction $\sqrt{3/2}\,\xi R_{nl}(\xi, z)$ can be evaluated accurately by the 3-point finite difference formulae (where n is the principal quantum number).

It has been demonstrated that the variable transformation greatly improves the accuracy (or helps the reduction in the number of grid points). To adjust the wave function to the steep rise of the Coulomb potential near the origin, grid points must be close together near the origin; to save computational effort, grid points must be gradually parted from each other at larger distances. The process of changing the step size can be carried out by transforming the linear scale variables x, y, and z to new variables. For the generalized cylindrical coordinate system of $\lambda = \frac{3}{2}$, the linear scale variable is ρ and the new variable is $\xi\ (=\rho^{2/3})$. Inverting the equally spaced ξ points onto linear scale ρ space, we find that this coordinate system possesses the desired feature that the spacing in linear scale coordinate ρ increases with increasing ρ. This is another benefit from the choice of $\lambda = \frac{3}{2}$.

4. NUMERICAL RESULTS AND DISCUSSION

A. *Error Definitions*

For the discussion of the efficiency and accuracy of the time propagation method presented in Section 3, we calculate the errors in amplitude and phase of the time-evolved wave function. Using the amplitude a_j and the phase ϕ_j of the wave function ψ_j at the point r_j,

$$\psi_j = a_j e^{i\phi_j}, \tag{25}$$

we introduce three amplitude-weighted errors defined as

$$\sigma_A^2 = \sum_j a_{R,j}^2 \left(\frac{a_j - a_{R,j}}{a_{R,j}}\right)^2 \Bigg/ \sum_j a_{R,j}^2, \tag{26}$$

$$\sigma_P^2 = \sum_j a_{R,j}^2 (\phi_j - \phi_{R,j})^2 \Bigg/ \sum_j a_{R,j}^2, \tag{27}$$

$$\sigma_\psi^2 = \sum_j a_{R,j}^2 \left|\frac{\psi_j - \psi_{R,j}}{a_{R,j}}\right|^2 \Bigg/ \sum_j a_{R,j}^2, \tag{28}$$

where "R" stands for the reference value and σ_A, σ_P, and σ_ψ represent the amplitude error, the phase error, and the absolute value of the difference between ψ and ψ_R, respectively. The phase difference $\phi_j - \phi_{R,j}$ is defined as the angle between the two phases that is smaller than π. These three errors are approximately related as

$$\sigma_\psi^2 \approx \sigma_A^2 + \sigma_P^2. \tag{29}$$

The quality of the wave function in momentum space should be checked by comparing its Fourier spectrum with the exact one. We here make do with calculating the average kinetic energy $\langle K \rangle$ to avoid repeating Fourier transforms. We use σ_K defined as

$$\sigma_K = \frac{\langle K \rangle - \langle K \rangle_R}{\langle K \rangle_R}, \tag{30}$$

where $\langle K \rangle_R$ denotes the reference value. The σ_K can be an oscillating function of time; it takes positive and negative values. When in this paper we give log σ_K, it is the logarithm of the envelope function of σ_K.

B. *Numerical Stability for the 1s Stationary State*

To examine the numerical stability and accuracy of our method, we first apply it to the stationary case where no laser field is applied and the atom is initially (at $t = 0$) in the ground state 1s (for which the transformed wave function is $\psi_{1s} = \sqrt{3}\xi e^{-r}$). It should be noted that the grid representation of the analytic wave function ψ_{1s} of the field-free differential Hamiltonian, ψ_{1s}^f, is not identical with the ground state of the discretized Hamiltonian, ψ'_{1s}. The ψ_{1s}^f includes excited state components $\{\psi'_j\}$ of the discretized Hamiltonian, i.e., $\psi_{1s}^f = \sum c_j \psi'_j$, where j runs from 1s (c_{1s} is domainant). The time evolution of ψ_{1s}^f is given by our method as $\psi_{1s}^f(t) \approx \sum c_j \psi'_j \exp(-itE'_j)$, where E'_j are eigenvalues of the discretized Hamiltonian.

The difference between ψ_{1s}^f and ψ'_{1s} is, in the following cases, so small ($c_{1s} \approx 1$) that the existence of spurious excited state components does not blur the discussions. We therefore do not eliminate the spurious excited states, although it is possible to generate the discretized ground state ψ'_{1s} either by diagonalizing the discretized Hamiltonian or by integrating the discretized form of the Schrödinger equation in imaginary time [30].

The reference values taken are those of the grid representation of the analytic time evolution function $\psi_{1s}(t) =$

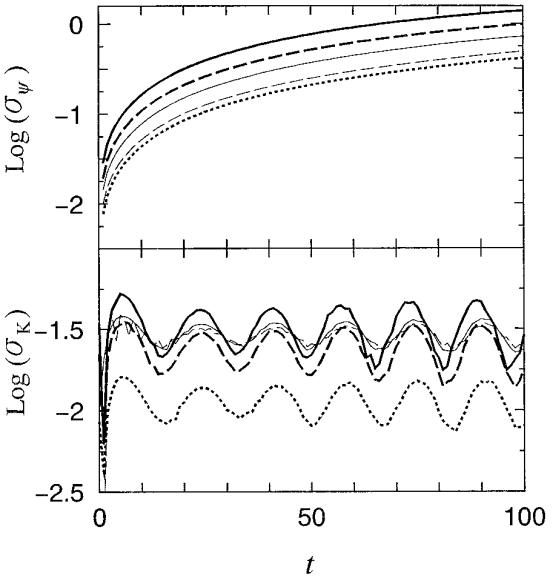

FIG. 1. Time variations in the errors σ_ψ and ϕ_K for the 1s state. The errors for $\Delta z = \Delta\xi = 0.1, 0.08, 0.05$ (in atomic units) are designated by the bold solid, broken, and dotted lines, respectively. The thin solid and broken lines designate the errors for $\Delta\xi = 0.05$ and $\Delta\xi = 0.025$, respectively ($\Delta z = 0.1$). The grid boundary is chosen as $z_{max} = 50.0$ and $\xi_{max} = 14$ (corresponding to 52.4 in the linear scale grid end ρ_{max}). The time step used is $\Delta t = 0.05$.

$\sqrt{3}\xi e^{-r} \exp(-itE_{1s})$. The errors σ_ψ and σ_K calculated are plotted in Fig. 1 as functions of time. The time step used is $\Delta t = 0.05$. The grid boundaries are chosen as $z_{max} = 50.0$ and $\xi_{max} = 14$ (corresponding to 52.4 in the linear scale grid end ρ_{max}). The three bold lines denote errors for the case where the grid spacings Δz and $\Delta\xi$ are taken to be the same; the bold solid, broken, and dotted lines indicate the errors for $\Delta z = \Delta\xi = 0.1, 0.08, 0.05$, respectively. Note that in these cases the number of grid points in ξ-space, N_ξ, is less than one-third (28/100) of that in the half range of z-space, N_z. The errors decrease monotonically with decreasing Δz and $\Delta\xi$. When Δz and $\Delta\xi$ decrease from 0.1 to 0.05, both σ_ψ and σ_K are reduced to one-third. The use of shorter Δt does not lead to applicable reduction in the errors, which indicates that the phase and amplitude errors for the parameters used in Fig. 1 are mainly due to the coarse discretizations in space (not due to the time discretizastion).

The phase error σ_P is nearly equal to σ_ψ (except where t is near 0). The amplitude error σ_A is much smaller than σ_ψ and is almost independent of time. Between $t = 0$ and $t = 100$, $\log \sigma_A$ is about -1.5 for $\Delta z = \Delta\xi = 0.1$ (the bold solid line case) and -2.0 for $\Delta z = \Delta\xi = 0.05$ (the bold dotted line case). For a stationary state, σ_A is small (i.e., $\sigma_\psi \approx \sigma_P$) and does not grow as rapidly as σ_ψ. This indicates that the time evolution of ψ^f_{1s} given by our method is approximately expressed as $\psi'_{1s} \exp(-itE'_{1s})$. Since $\psi^f_{1s}(t) \approx \psi'_{1s} \exp(-itE'_{1s})$ and $\psi_{1s}(t) = \psi_{1s} \exp(-itE_{1s})$, σ_A is determined by the small amplitude difference $\psi'_{1s} - \psi_{1s}$, which is independent of time. On the other hand, σ_P grows as $(E'_{1s} - E_{1s})t$ (the difference $E'_{1s} - E_{1s} \approx 10^{-2.5}$ for the bold dotted line case). This is the reason why σ_P becomes dominant in σ_ψ.

The kinetic energy error σ_K is nearly independent of time but shows beats of small amplitude. These features are explained by the form of $\psi^f_{1s}(t) \approx c_{1s}\psi'_{1s} \exp(-itE'_{1s}) + c_{2s}\psi'_{2s} \exp(-itE'_{2s})$, where $c_{1s} \approx 1$ and c_{2s}, i.e., the amount of the spurious excited state ψ'_{2s}, is much smaller than 1. The beats come from the interference between ψ'_{1s} and ψ'_{2s}; the beat frequency is identical with the difference $E'_{2s} - Ec'_{1s} \approx E_{2s} - E_{1s}$.

As mentioned in Section 3, the variable ξ possesses the desired feature that the corresponding spacing in linear scale coordinate ρ increases with increasing ρ. The value of N_ξ necessary for calculation of high precision is therefore expected to be smaller than N_z. The ratio 0.28:1 of N_ξ to N_z may, however, be too small (considering that the linear lengths z_{max} and ρ_{max} are nearly equal). To check the balance between N_ξ and N_z, $\Delta\xi$ is reduced while keeping the value of Δz constant. The errors for $\Delta\xi = 0.05$ and 0.025 are designated by the thin solid and broken lines, respectively ($\Delta z = 0.1$ as in the case designated by the bold solid line). As $\Delta\xi$ becomes smaller, σ_ψ and σ_K decrease but the reductions in the errors shrink, especially in σ_K (note the small difference in σ_K between the thin solid and broken lines). It is computationally inefficient and unnecessary to decrease the ratio $\Delta\xi/\Delta z$ below 0.5 (this is the ratio when $\Delta\xi = 0.05$ and $\Delta z = 0.1$).

The conventional method using the cylindrical coordinate ($\lambda = 1$) were also examined. To make a comparison with the $\lambda = \frac{3}{2}$ case, we chose the boundary condition and time step for the $\lambda = 1$ case to be the same as in Fig. 1; $z_{max} = 50.0$, $\rho_{max} = 52.4$ (equivalent to $\xi_{max} = 14$). For instance, when the numbers of grid points are the same as in the bold dotted line case (i.e., $N_z = 1000$ and $N_\rho = 280$), the errors σ_ψ and σ_K for $\lambda = 1$ are larger than those of the bold dotted line by a factor of more than 10. The difference $E'_{1s} - E_{1s}$ is about 10^{-1} (where E'_{1s} is the ground state energy of the discretized Hamiltonian for $\lambda = 1$). In addition, the global features of the 1s wave function are not conserved. Owing to the spurious excited states in the discretized wave function a wave propagates along the ρ-axis (around $z = 0$), breaking the isotropy of the 1s wave function. These drawbacks originate from the fact that the finite difference formula does not work for $\lambda = 1$ (as mentioned in Section 3).

C. *Time Evolution of the 1s + 2p$_z$ Nonstationary State*

We next compute the time evolution of the grid representation of the analytic function $(1s + 2p_z)/\sqrt{2}$. The

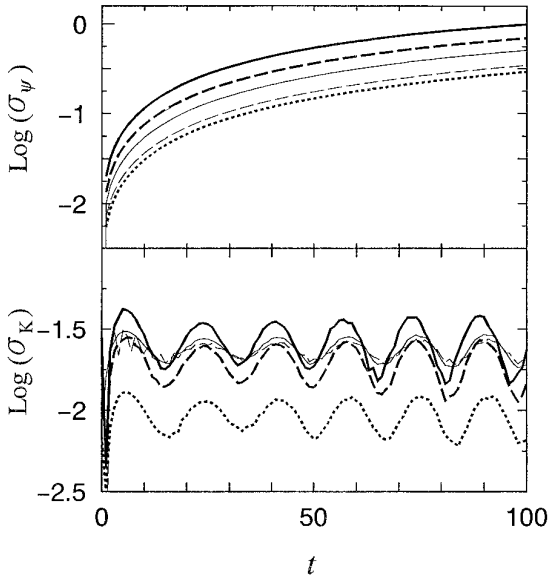

FIG. 2. Time variations in the errors σ_ψ and σ_K for the 1s + $2p_z$ state. The notations are the same as in Fig. 1 (the time step and the grid boundaries are also the same as in Fig. 1).

reference time evolution is given by $\psi(t) = \sqrt{3/2}\xi[e^{-r} \times \exp(-iE_{1s}t) + (1/4\sqrt{2})z\, e^{r/2} \exp(-iE_{2s}t)]$. The errors σ_ψ and σ_K are plotted in Fig. 2. The notations for lines are the same as in Fig. 1 (so are the time step and the grid boundaries). The errors are a little smaller for 1s + $2p_z$ than for 1s. As the average of radial coordinate r becomes larger, the steep rise of the Coulomb potential around the origin damages the accuracy less severely. In this sense, the time evolution of the 1s state is the most difficult to deal with. Since the exact propagation of the 1s state is known, as shown in Section 4B, one can determine the time step Δt and the grid spacings $\Delta\xi$ and Δz that achieve the desired accuracy in the time evolution of the 1s state. The values of parameters determined can be generally used for the time evolution of excited states, e.g., for the case where the atom interacts with a laser pulse.

The σ_A is an oscillating function of time, unlike in the 1s case, but it is still smaller than σ_P. The time evolution given by our method is approximately expressed as $[\psi'_{1s} \times \exp(-itE'_{1s}) + \psi'_{2p} \exp(-itE'_{2p})/\sqrt{2}$. This describes the features of σ_A and σ_P. The beats in σ_K is due to the spurious excited state ψ'_{2s} and is not due to the interference between ψ'_{1s} and ψ'_{2p}. There is no such interference because $\langle\psi_{1s}|K_\xi + K_z|\psi_{2p}\rangle = 0$.

D. *Consistency and Stability*

The numerical results presented suggest that convergence to the solution of the Schrödinger equation can be obtained by reducing the spacings Δz, $\Delta\xi$, and Δt. First, we check the consistency of our method with the Schrödinger equation and then examine the stability. The consistency is clarified by expanding the finite difference representation of Eq. (24) around $t = t_n$:

$$\begin{aligned} i\frac{\partial\psi}{\partial t} - H(t)\psi = &-\frac{i\,\Delta t^2}{24}\left(\frac{\partial^3\psi}{\partial^3 t} + 3iH(t)\frac{\partial^2\psi}{\partial^2 t}\right) \\ &+ \frac{i\,\Delta t^2 B(t)A(t)}{4}\frac{\partial\psi}{\partial t} - \frac{\Delta z^2}{24}\frac{\partial^4\psi}{\partial z^4} \\ &- \frac{\Delta\xi^2}{24\lambda^2\xi^{2\lambda}}\left(\xi^2\frac{\partial^4\psi}{\partial\xi^4} - 4(\lambda-1)\xi\frac{\partial^3\psi}{\partial\xi^3}\right) + \cdots . \end{aligned} \tag{31}$$

Our finite difference scheme is accurate up to the order of Δz^2, $\Delta\xi^2$, and Δt^2. The scheme agrees with the Schrödinger equation by reducing the spacings independently without constraints; that is, it is unconditionally consistent with the Schrödinger equation. This ensures that the solution of our method converges to that of the Schrödinger equation by reducing Δz, $\Delta\xi$, and Δt on the condition that the method is numerically stable; i.e., the error does not grow exponentially with time.

The approximate propagator Eq. (24) used here is unitary so that the norm is strictly conserved. It should be, however, noted that the operation of the Hamiltonian (18) on the wave function is evaluated approximately by the finite difference formula. For the normalization condition given by (16), if the tridiagonal matrix resulting from the finite difference representation of K_ξ were symmetric with respect to grid points $\xi_j = j\,\Delta\xi$, the norm would be conserved; in fact, the tridiagonal matrix is only approximately symmetric. The ratio of the matrix element $\langle j+1|K_\xi|j\rangle$ to $\langle j|K_\xi|j+1\rangle$ is, for the 3-point finite difference used,

$$\begin{aligned} 1 + \frac{\Delta\xi}{2\xi_{j+1}} : \frac{1}{\left(1 - \dfrac{\Delta\xi}{\xi_{j+1}}\right)} - \frac{\Delta\xi/\xi_{j+1}}{2\left(1 - \dfrac{\Delta\xi}{\xi_{j+1}}\right)^2} = 1 \\ + \frac{\Delta\xi}{2\xi_{j+1}} : 1 + \frac{\Delta\xi}{2\xi_j} - \frac{\Delta\xi^3}{2\xi_{j+1}^3} + O\left(\frac{\Delta\xi^4}{\xi_{j+1}^4}\right). \end{aligned} \tag{32}$$

As $\Delta\xi/\xi_{j+1}$ decreases, the tridiagonal matrix becomes symmetric. For $j = 1$ (the next point to the origin), the ratio between the above matrix elements is $1 : \frac{4}{5}$; for $j = 2$, the ratio is $1 : \frac{27}{28}$.

We next demonstrate numerically how much the norm and overlap of the 1s state decrease with time. Four cases are shown in Fig. 3: $\Delta z = \Delta\xi = 0.1$ (solid); $\Delta z = 0.05$ and $\Delta\xi = 0.1$ (dash-dotted); $\Delta z = 0.1$ and $\Delta\xi = 0.05$ (broken); $\Delta z = \Delta\xi = 0.05$ (dotted). The time step and the grid boundaries are the same as in Fig. 1. The calculated norm is designated by the bold line and the absolute value of

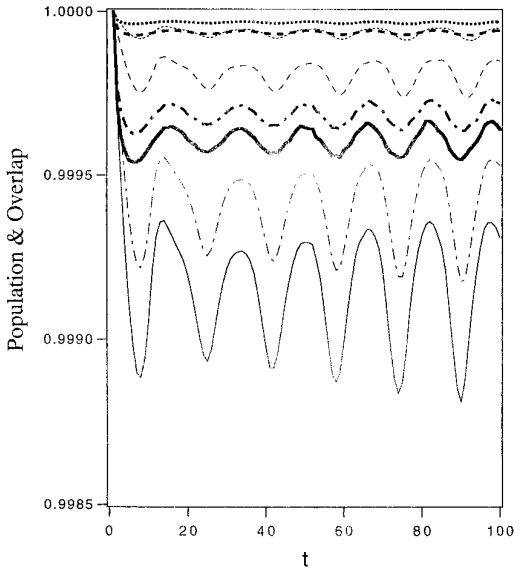

FIG. 3. The 1s norm and overlap calculated for four cases: $\Delta z = \Delta\xi = 0.1$ (solid); $\Delta z = 0.05$ and $\Delta\xi = 0.1$ (dash-dotted); $\Delta z = 0.1$ and $\Delta\xi = 0.05$ (broken); $\Delta z = \Delta\xi = 0.05$ (dotted). The calculated norm is designated by the bold line and the absolute value of the overlap between the exact 1s state and the calculated 1s state (evolving in time) is designated by the thin line. The time step and the grid boundary are the same as in Fig. 1.

the overlap between the 1s grid representation $\psi^{\mathrm{f}}_{1\mathrm{s}}$ and the time evolved state $\psi^{\mathrm{f}}_{1\mathrm{s}}(t)$ is designated by the thin line.

The absolute value of the overlap is smaller than the norm but very close to it. The decrease of the overlap is much smaller than anticipated from the large phase error in Fig. 1, indicating that the large phase difference $\phi_j - \phi_{\mathrm{R},j}$ is nearly uniform in space. This is in accord with the fact that the phase error σ_{P} which grows as $(E'_{1\mathrm{s}} - E_{1\mathrm{s}})t$ is independent of the grid positions. If the state is stationary like 1s, the phase error tends to be uniform. On the other hand, for nonstationary states, the quality of the overlap is deteriorated because of the nonuniform distribution of phase error.

The norm of the grid representation $\psi^{\mathrm{f}}_{1\mathrm{s}}$ is smaller than 1 at $t = 0$ and then decreases to oscillate. The leakage of norm is much smaller than the amplitude error σ_{A}. To define the norm precisely, $\psi^{\mathrm{f}}_{1\mathrm{s}}(t = 0)$ should be multiplied by the renormalization constant c_{N} so that $c^2_{\mathrm{N}} \langle \psi^{\mathrm{f}}_{1\mathrm{s}} | \psi^{\mathrm{f}}_{1\mathrm{s}} \rangle = 1$. The leakage is defined as the difference between 1 and the norm of $c_{\mathrm{N}}\psi^{\mathrm{f}}_{1\mathrm{s}}(t)$.

For the reduction in Δz, the norm is not improved as much as the overlap (cf. the bold solid and dash-dotted lines, or cf. the bold broken and dotted lines). The dependence of the leakage on Δz is weak because the finite difference formula for K_z is symmetric. On the other hand, from the comparison between the solid and broken line cases or from the dash-dotted and dotted line cases (which have the same value of Δz but have different values of $\Delta\xi$), we find that the leakage depends strongly on $\Delta\xi$, as anticipated. The leakage approaches zero as $\Delta\xi$ becomes smaller, which reflects the fact that the tridiagonal matrix becomes symmetric with decreasing $\Delta\xi$. For excited states, whether stationary or not, the conservation of the norm is rather good in comparison with the 1s case, which reflects the fact that the asymmetric part becomes negligible for large ξ_j. For the grid spacings used in the solid line case, the leakage of 1s is about 5×10^{-4} but the leakage of $2\mathrm{p}_z$ is less than 10^{-5}. The norm is conserved to the extent of the validity of the finite difference formula employed.

The question left is whether the stability of our method is conditional or unconditional. Extensive investigation by changing the parameters in a wide range reveals that our method is conditionally stable. The stability condition obtained by the numerical investigation is shown in Fig. 4 (although the von Neumann analysis [17, 31] suggests that the stability of the method is conditional, we could not analytically derived the condition). Each thin line gives the stability condition imposed on $\Delta\xi$ and Δt when Δz is fixed at a value; the solid, broken, dash-dotted, and dotted lines give the borders for $\Delta z = 0.1$, 0.08, 0.05, and 0.025, respectively. Our method is stable if the values of $\Delta\xi$ and Δt lie in the region below the border.

For the typical case where $\Delta z = \Delta\xi$, the upper limit of Δt for which the method is stable is given by the closed dots in Fig. 4. They can be fitted by the quadratic function $\Delta t = 1.8$

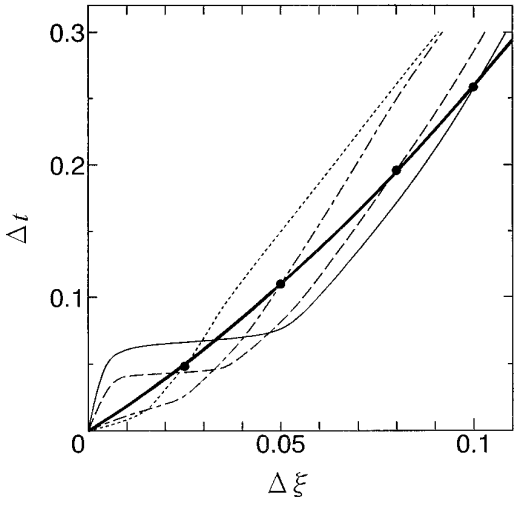

FIG. 4. The stability condition obtained by the numerical investigation. Each thin line gives the stability condition imposed on $\Delta\xi$ and Δt when Δz is fixed at a value; the solid, broken, dash-dotted, and dotted lines give the borders for $\Delta z = 0.1$, 0.08, 0.05, and 0.025, respectively. Our method is stable if the values of $\Delta\xi$ and Δt lie in the region below the border. For the typical case where $\Delta z = \Delta\xi$, the upper limit of Δt required for stability is given by the closed dots which can be fitted by the quadratic function $\Delta t \approx 1.8\,\Delta\xi + 0.8\,\Delta\xi^2$ (denoted by the bond line).

$\Delta\xi + 0.8\,\Delta\xi^2$ denoted by the bold line. This stability condition, however, does not give severe restrictions; it is fulfilled for the reasonable values of parameters, as has been shown in Figs. 1 to 3. For moderate values of Δz and $\Delta\xi$ (>0.025), Δt can be as large as 0.05. When extremely small values of Δz and $\Delta\xi$ (<0.025) are needed to achieve high precision in calculation, the stability condition requires that Δt should be smaller than 0.05. This is, however, not an extra requirement. When small values of Δz and $\Delta\xi$ (<0.025) are needed, the time discretization Δt must be as fine as the space discretizations, as is known from Eq. (31). Reconciliation between stability and efficiency leads to the standard choice that $\Delta z = \Delta\xi$ and $\Delta t = 1.8\,\Delta\xi + 0.8\,\Delta\xi^2$. By reducing $\Delta\xi$, Δz, and Δt while keeping these relations, the errors in calculation can be reduced to desired precision.

E. *Dynamics of the Hydrogen Atom Reacting to a Linearly Polarized Strong Laser Pulse*

An example of the dynamics of the hydrogen atom interacting with a z-polarized pulse is shown in Fig. 5. A series of wave functions from $t = 0$ to $t = 60$ is given. The initial state at $t = 0$ is the 1s.The absolute value of the wave function, $\sqrt{2}|R(t)|$, is plotted as a function of cylindrical coordinates ρ and z (the packet is symmetrical about the z-axis). Although at $t = 0$ the peak height of $\sqrt{2}|R|$ is 2, the wave functions shown in Fig. 5 are truncated at $\sqrt{2}|R| = 0.01$ to depict the ionization process in detail.

The electric field of the pulse is assumed to have the envelope

$$\mathscr{E}(t) = \mathscr{E}_0 \sin^2(\pi t/T_p) \quad \text{for } 0 \le t \le T_p; \qquad \text{otherwise,} \quad \mathscr{E}(t) = 0, \tag{33}$$

where T_p is the pulse duration. The parameters of the pulse are in atomic units: $T_p = 40$ ($\approx$1fs), $\omega = 0.75$, $\mathscr{E}_0 = 0.1$ ($=5.1 \times 10^{10}$V m^{-1} which amounts to 3.5×10^{14}W cm^{-2}). The amplitude of the electric field is plotted in Fig. 6. The arrow in each panel of Fig. 5 denotes the direction of the electric force at each time. The other parameters used are as follows: $\xi_{max} = 27$ and $\Delta\xi = 0.07$ ($N_\xi = 385$); $z_{max} = 65$ and $\Delta z = 0.1$ ($N_z = 650$); $\Delta t = 0.05$.

Around $t = 10$, the wave function is squeezed in comparison with the 1s and is encircled by a low ridge around $r = 10$. The wave function then starts spreading while it is squeezed on the side where the electron is pushed toward the nucleus by the electric force (when $\mathscr{E}(t) > 0$ it is the side where $z > 0$) and it is stretched on the other side. While the wave function on each side undergoes the squeezing force and the opposite force alternately, an outgoing component is tone from each side of the core. The wave function begins to split around $t = 20$. It is clearly seen around $t = 30$ that the wave function is cloven on the negative z side of the core. At the end of the pulse ($t = 40$), another lobe appears on the positive z side. Although for the period from $t = 30$ to $t = 40$ the electric field that stretches the wave function on the positive z side is much weaker than those around $t = 20$, a cleavage occurs on the positive z side during the period.

As the panel at $t = 60$ shows, the two lobes go outward [9, 32]. To avoid reflections from the outer grid boundary $z = \pm z_{max}$ and $\xi = \xi_{max}$, an appropriate absorbing boundary is imposed (the outgoing waves near the outer boundary are multiplied by a mask function that gradually decreases from 1 toward 0). Around $t = 160$, the ionizing wave has completely gone out of the range drawn in the panel. The probability of ionization which can be obtained by subtracting the bound component left from the initial population is about 0.025 and the remaining component is the 1s of a population of 0.975. The ionization probability does not decrease by increasing the grid ends ξ_{max} and z_{max} (while keeping $\Delta\xi$ and Δz constant), which indicates that in this case excited bound states are hardly populated.

5. CONCLUSIONS

In this paper, we have presented a method whereby the 3D dynamics of the electronic wave packet in a hydrogen atom can be calculated efficiently. Our method is constructed so as to satisfy the following three requirements: (i) the normalization condition (16) is fulfilled; (ii) the transformed wave function used is zero at the Coulomb singular point so that the numerical difficulties concerning the singularity are avoided; (iii) the coordinate system is chosen so that the differential operators in the Hamiltonian can be well evaluated by the 3-point finite difference formula even near the singular point. The time-dependent Schrödinger equation represented in terms of the transformed wave function and the corresponding Hamiltonian is discretized in time and space, and then solved by the PR method. The discretized scheme is proved to be unconditionally consistent with the Schrödinger equation. The way of starting from the normalization condition (16) is in a sense heuristic. We have no strong reason to exclude the other normalization conditions. We have tested other normalization conditions, but all the propagation schemes derived were unstable or less accurate, for the present.

The generalized cylindrical coordinate system (ξ^λ, z, φ) is used to satisfy the conditions (ii) and (iii), and the value of λ is determined to be $\frac{3}{2}$. The variable ξ in the generalized cylindrical coordinate system of $\lambda = \frac{3}{2}$ is related with the linear scale variable ρ as $\xi = \rho^{2/3}$. The use of ξ variable satisfies the condition desired for the Coulomb potential; discretizing ξ space at equal intervals is equivalent to discretizing ρ space so that the spacing $\Delta\rho$ increases with increasing ρ. The number of grid points in ξ-space, N_ξ, necessary for calculation of high accuracy is smaller than that in the half range of z-space, N_z (note that z is a linear

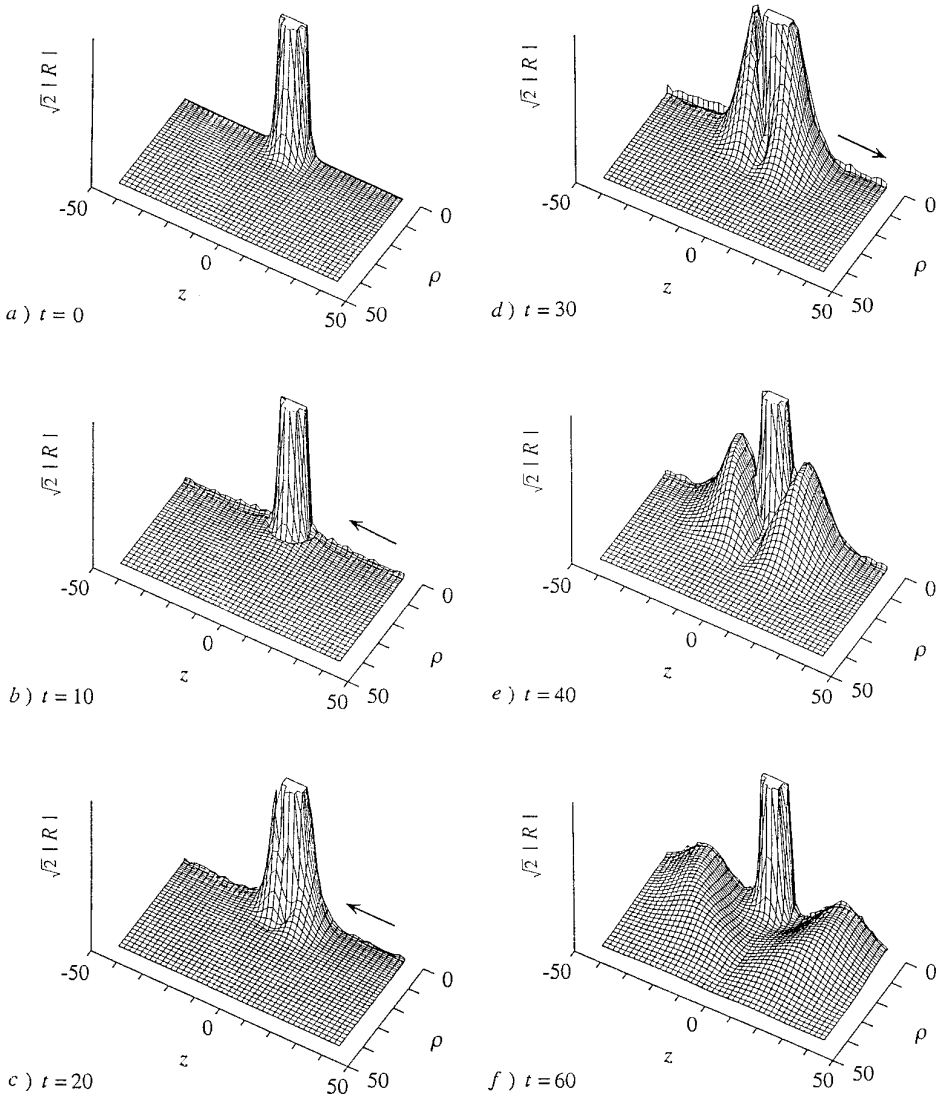

FIG. 5. An example of the dynamics of the hydrogen atom interacting with a z-polarized pulse. The absolute values of wave functions, $\sqrt{2}|R(t)|$, are represented in cylindrical coordinates ρ and z. The initial state is the 1s. The amplitude of the electric field is plotted in Fig. 6. The other parameters used are as follows: $\xi_{\max} = 27$, $\Delta\xi = 0.07$; $z_{\max} = 65$, $\Delta z = 0.1$; $\Delta t = 0.05$. The direction of the electric force at each time is denoted by an arrow.

scale coordinate). N_ξ can be one-third as large as N_z. The introduction of the ξ variable helps the reduction in the number of grid points.

To examine the numerical stability and accuracy of our method, we have applied it to cases where no laser field is turned on. The wave functions calculated by our method are compared with the exact ones to estimate the errors. It turns out that our method is superior to the method using the ordinary cylindrical coordinate ($\lambda = 1$). For $\lambda = 1$, the errors σ_ψ and σ_K are more than 10 times as large as those for $\lambda = \frac{3}{2}$ and the phase error is not uniform in space (the 1s overlap is reduced to 0.9 for the solid line case in Fig. 3). These drawbacks originate from the fact that the finite difference formula does not work for $\lambda = 1$.

The norm is not strictly conserved for $\lambda = \frac{3}{2}$, although the analytic form of the approximate propagator Eq. (24) is unitary. The reason is that the operation of the Hamiltonian (18) on the wave function is approximated by the finite difference formula. Under the normalization condition (16), the conservation of norm means that the tridiagonal matrix resulting from the finite difference representation of K_ξ is symmetric with respect to grid points $\xi_j = j\,\Delta\xi$; in fact, the tridiagonal matrix is only approximately symmetric. As a result, the norm is smaller than 1, but the leakage of norm is negligible. As $\Delta\xi/\xi_{j+1}$ decreases, the tridiagonal matrix becomes symmetric: the norm is conserved to the extent of the validity of the finite difference formula employed. For excited states, the conservation of

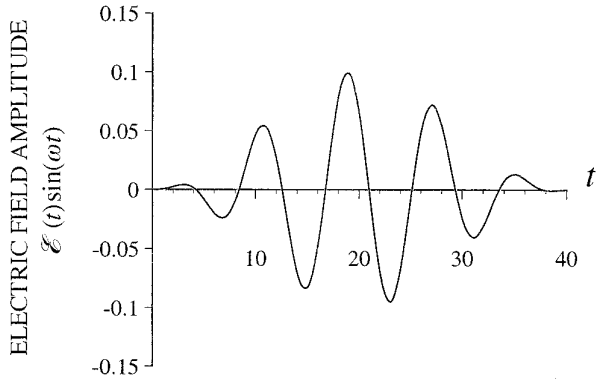

FIG. 6. The electric field amplitude of the pulse. The parameters of the pulse are in atomic units: the pulse duration $T_p = 40(\approx 1\text{fs})$, $\omega = 0.75$, the maximum field amplitude $\mathscr{E}_0 = 0.1$.

the norm is rather good in comparison with the 1s case, which reflects the fact that the asymmetric part becomes negligible for large ξ_j.

Convergence to the solution of the Schrödinger equation can be obtained by reducing Δz, $\Delta\xi$, and Δt when our method is stable, i.e., when the error does not grow exponentially with time. The stability of our method is conditional. For the typical case where $\Delta z = \Delta\xi$, the condition required for stability is that Δt should be smaller than $1.8\ \Delta\xi + 0.8\ \Delta\xi^2$, i.e., that Δt should be as small as the grid spacings. This stability condition does not impose an extra condition on Δt; when extremely small values of Δz and $\Delta\xi$ (<0.025) are needed to perform calculations of high accuracy, the time discretization Δt must be as fine as the space discretizations. Reconciliation between stability and efficiency leads to the standard choice that $\Delta z = \Delta\xi$ and $\Delta t = 1.8\ \Delta\xi + 0.8\ \Delta\xi^2$. Convergence to the solution of the Schrödinger equation is ensured by reducing the time and grid spacings while keeping these relations.

Our method is applicable to the case where the atom interacts with a linearly polarized laser pulse. For a variety of sets of pulse parameters, fully converged calculations are performed. We have illustrated a series of snapshots of the electronic wave packet that moves in real space while coherently interacting with a strong femtosecond pulse (of which peak field strength is $\mathscr{E}_0 = 0.1$). The mechanism of ionization can be analyzed in detail. In conclusion, our method is highly reliable and is a powerful tool of analyzing ionization processes including above threshold ionization and chaotic ionization of hydrogen atom. Application to H_2^+ is also possible. It is straightforward when the pulse is linearly polarized parallel with the internuclear axis (the z axis is chosen to be the internuclear axis) and the internuclear distance is fixed [33]. All we have to do is to replace the Coulomb interaction in Eq. (21) with the interaction between the electron and two nuclei. The dynamics of 1D nuclear motion restricted to the direction of the laser electric field can be incorporated into our scheme by using the ADI for three degrees of freedom, though it demands huge memory and much longer CPU time [34].

ACKNOWLEDGMENTS

We are indebted to the Japan Society for the Promotion of Science for support of the Japan–Canada joint research project "Control of Reaction Dynamics by Laser." We thank the participating scientists on the Canadian side, Professor A. D. Bandrauk, Dr. S. Chelkowski and Dr. T. Zuo for helpful discussions.

Note added in proof. The tridiagonal system of linear equations was solved by LU decomposition with pivoting. The numerical instability of our scheme turned out to be due to the pivoting. By avoiding the use of pivoting, practically, the method becomes unconditionally stable.

REFERENCES

1. J. H. Eberly, J. Javanainen, and K. Rzazewski, *Phys. Rep.* **204,** 331 (1991).
2. C. A. Nicolaides, C. W. Clark, and M. H. Nayfeh (Eds.), *Atoms in Strong Fields* (Plenum, New York, 1990).
3. A. D. Bandrauk (Ed.), *Molecules in Laser Fields* (Dekker, New York, 1994).
4. See papers in *Adv. At. Mol. Phys. Suppl.* **1** (1992).
5. G. Alber and P. Zoller, *Phys. Rep.* **199,** 231 (1991).
6. J. Javanainen, J. H. Eberly, and Q. Su, *Phys. Rev. A* **38,** 3430 (1988); J. H. Eberly, R. Grobe, C. K. Law, and Q. Su, *Adv. At. Mol. Phys. Suppl.* **1,** 301 (1992).
7. U. Schwengelbeck and F. H. M. Faisal, *Phys. Rev. A* **50,** 632 (1994); R.Dehnen and V. Engel, *Phys. Rev. A* **52,** 2288 (1995).
8. R. V. Jensen, S. M. Susskind, and M. M. Sanders, *Phys. Rep.* **201,** 1 (1991); G. Casati, B. V. Chirikov, and D. L. Shepelyansky, *Phys. Rep.* **154,** 77 (1987).
9. K. C. Kulander, K. J. Schafer, and J. L. Krause, *Adv. At. Mol. Phys. Suppl.* **1,** 247 (1992).
10. K. C. Kulander, *Phys. Rev. A* **35,** 445 (1987); K. C. Kulander, K. R. Sandhya Devi, and S. E. Koonin, *Phys. Rev. A* **25,** 2968 (1982).
11. M. S. Pindzola and M. Dörr, *Phys. Rev. A* **43,** 439 (1991).
12. H. Yu, A. D. Bandrauk, and V. Sonnard, *J. Math. Chem.* **15,** 273 (1994).
13. M. Dörr, O. Latinne, and C. J. Joachain, *Phys. Rev. A* **52,** 4289 (1995).
14. J. A. Fleck, Jr., J. R. Morris, and M. D. Feit, *Appl. Phys.* **10,** 129 (1976); M. D. Feit, J. A. Fleck Jr., and A. Steiger, *J. Comput. Phys.* **47,** 412 (1982).
15. H. Kono and S. H. Lin, *J. Chem. Phys.* **84,** 1071 (1986).
16. T. N. Truong, J. J. Tanner, P. Bala, J. A. McCammon, D. J. Kouri, B. Lesyng, and D. K. Hoffman, *J. Chem. Phys.* **96,** 2077 (1992).
17. W. H. Press, S. A. Teukolsky, W. T. Vetterling, and B. P. Flannery, *Numerical Recipes in Fortran,* 2nd ed. (Cambridge Univ. Press, New York, 1992), Chap. 19.
18. A. Askar and A. S. Cakmak, *J. Chem. Phys.* **68,** 2794 (1978).
19. R. Varga, *Matrix Iterative Analysis* (Prentice–Hall, Englewood Cliffs, NJ, 1962), p. 273.
20. S. E. Koonin, K. T. R. Davies, V. Maruhn-Rezwani, H. Feldmeier, S. J. Krieger, and J. W. Negele, *Phys. Rev. C* **15,** 1359 (1977).

21. N. N. Yanenko, *The Method of Fractional Steps* (Springer-Verlag, New York, 1971).
22. A. R. Mitchell, *Computational Methods in Partial Differential Equations* (Wiley, New York, 1969).
23. A. Kita, H. Kono, Y. Ohtsuki, and Y. Fujimura, to be published.
24. C. Froese Fischer, *The Hartree-Fock Method for Atoms* (Wiley, New York, 1976), p. 223.
25. E. Trefftz, A. Schlüter, K-H. Dettmar, and K. Jörgens, *Z. Astrophys.* **44,** 1 (1957).
26. L. V. Chernysheva, N. A. Cherepkov, and V. Radojević, *Comput. Phys. Commun.* **11,** 57 (1976).
27. The polar coordinate system has been also used. See, for example, Refs. [12, 13].
28. E. A. McCullogh and R. E. Wyatt, *J. Chem. Phys.* **54,** 3578 (1971); **54,** 3592 (1971).
29. The 3-point finite difference formula for the first derivative is $[\psi(\xi + \Delta\xi, z) - \psi(\xi - \Delta\xi, z)]/2\,\Delta\xi$.
30. Thereby, the spurious excited states are eliminated and only the ground state survives (the relaxation method). See, for example, H. Flocard, S. E. Koonin, and M. S. Weiss, *Phys. Rev. C* **17,** 1682 (1978); R. Kosloff and H. Tal-Ezer, *Chem. Phys. Lett.* **127,** 223 (1986).
31. G. G. O'Brien, M. A. Hyman, and S. Kaplan, *J. Math. Phys.* **29,** 223 (1951).
32. M. Gavrila, *Adv. At. Mol. Phys. Suppl.* **1,** 435 (1992).
33. Using the cylindrical coordinate system, Zuo *et al.* have treated the problem. See, for example, T. Zuo, A. D. Bandrauk, M. Ivanov, and P. B. Corkum, *Phys. Rev. A* **51,** 3991 (1995).
34. The problem has been challenged in S. Chelkowski, T. Zuo, O. Atabek, and A. D. Bandrauk, *Phys. Rev. A* **52,** 2977 (1995).